Electronic Supplementary Information

Accelerating interfacial charge transfer and photocatalytic activity of Z-scheme Zn-MOF/GO heterojunction towards the removal of Cr(VI) and methylene blue

Qiang Chen[a], Chenzhu Zhao[a], Xusheng Li[a], Hua Liu[a], Jiao Chen[a], Quanquan Li[a,b,*], Ping Liu[a,*], and Yaoyu Wang[a]

[a] *College of Chemistry & Materials Science, Northwest University, Xi'an 710127, P. R. China.*

[b] *College of New Energy, Yulin University, Shaanxi Province, Yulin 719000, P. R. China.*

*Corresponding Authors

E-mail: P. Liu (liuping@nwu.edu.cn)

Q. Li (liquanquan122@163.com)

Content

1. Experimental section

1.1 Materials

All the solvents and reagents employed in this work are purchased and they need not further treatment. Graphene oxide (GO) we use was prepared by the exfoliation of graphite oxide. Throughout this process, graphite oxide was homogeneously dispersed in deionized water and kept in ultraphonic treatment for 6 h. The uniform and stable slightly brown liquid was obtained and sealed reserve for use. (2,2′-bipyridine)-3,3′-dicarboxylic acid, 1,1′-dioxide (H_2L, 97%) and 4,4'-vinylenedipyridine (bpe, 98%) were purchased from Le Yan Chemical Co., Ltd. (China). Zinc nitrate hydrate ($Zn(NO_3)·6H_2O$, 98%), Potassium hydroxide (KOH, 85%), Methanol (CH_3OH, 99.5%), were purchased from Fu Yu Chemical Reagent Co. Ltd. (China). Moreover, deionized water was used in the whole experiment. Thermogravimetric analyses (TGA) are tested on a NETZSCH TG209F3 under a N_2 atmosphere between 30 and 800°C (heating rate: 10°C min^{-1}). The powder X-ray diffraction patterns (PXRD) are tested applying a Bruker D8 ADVANCE X-ray powder diffractometer (Cu−Kα, 1.5418Å). Luminescence spectra are determined on a PerkinElmer LS55 luminescence spectrometer (for solid state) and a Hitachi F-4500 fluorescence spectrophotometer (for ethanol suspension state) at room temperature. Luminescent lifetime was recorded on an Edinburgh FLsp920 with excitation at 250 nm. UV-vis diffuse reflectance spectroscopy (DRS) was performed by using a UV-3600 PLUS UV-vis spectrophotometer, during which $BaSO_4$ was adopted as the internal reflectivity standard. The morphology was observed on a JSM-7001F field emission scanning electron microscope (FE-SEM). The Mott–Schottky, it and EIS analysis was performed on an electrochemical workstation (chi660e). The UV/visible spectra were recorded with a U-3310 spectrophotometer.

1.2 X-ray data collection and structure determination

Single crystal X-ray diffraction analyses are operated on a Bruker D8 VENTURE PHOTON II diffractometer with graphite monochromated Ga-Kα radiation (λ = 1.34139 Å) at *ca.* 298 K. The structure of MOF was analyzed and refined *via* direct and full-matrix least-squares method on F^2 with anisotropic thermal parameters for all non-hydrogen atoms (SHELXL-97), respectively. Hydrogen atoms are placed in calculated positions and treated with a riding method. Further details of structural analyses of Zn-MOF is recorded in Table S1. Selected bond lengths and angles are

listed in Table S2.

Table S1 Crystallographic data of $Zn^{L\text{-bpe}}$

MOF	$Zn^{L\text{-bpe}}$
chemical formula	$C_{48}H_{34}N_8O_{21}Zn_3$
CCDC	2338673
formula weight	1254.94
crystal shape	block
crystal color	colorless
temperature (K)	100
crystal system	Monoclinic
space group	C12/c1
a/Å	14.3702(8)
b/Å	13.3514(8)
c/Å	24.3154(14)
α (°)	90
β (°)	94.535(2)
γ (°)	90
V/Å^3	4650.6(5)
Z	4
density (mg/m^3)	1.792
μ (mm^{-1})	1.743
F(000)	2544
R_{int}	0.0436
Goof	1.039
$R_1{}^a$,$wR_2{}^b$[I>2σ(I)]	0.0300, 0.0757
R_1, wR_2 (all data)	0.0355, 0.0788

$^a R_1 = \Sigma||F_o|-|F_c||/\Sigma|F_o|$; $^b wR_2 = [\Sigma w(F_o{}^2 - F_c{}^2)^2/\Sigma w(F_o{}^2)^2]^{1/2}$

Table S2 The selected bond lengths (Å) and angles (°) for $Zn^{L\text{-bpe}}$

$Zn^{L\text{-bpe}}$			
Zn(1)-O(1)#1	2.1161(1)	Zn(1)-O(1)	2.1160(1)
Zn(1)-O(4)#1	2.0938(2)	Zn(1)-O(4)	2.0938(2)
Zn(1)-O(8)#2	2.1161(2)	Zn(1)-O(8)#3	2.1161(2)
Zn(2)-O(3)	1.9469(2)	Zn(2)-O(6)#4	2.0041(1)
Zn(2)-O(10)	1.9452(2)	Zn(2)-N(3)	2.0384(2)

O(1)-Zn(1)-O(1)#1	178.71(8)	O(1)#1-Zn(1)-O(8)#3	91.95(5)
O(1)-Zn(1)-O(8)#3	88.94(5)	O(1)#1-Zn(1)-O(8)#2	88.95(5)
O(1)-Zn(1)-O(8)#2	91.95(5)	O(4)-Zn(1)-O(1)	85.06(5)
O(4)-Zn(1)-O(1)#1	93.99(5)	O(4)#1-Zn(1)-O(1)#1	85.06(5)
O(4)#1-Zn(1)-O(1)	93.99(5)	O(4)-Zn(1)-O(4)#1	85.90(8)
O(4)-Zn(1)-O(8)#3	90.82(6)	O(4)#1-Zn(1)-O(8)#3	175.39(6)
O(4)#1-Zn(1)-O(8)#2	90.82(6)	O(4)-Zn(1)-O(8)#2	175.39(6)
O(8)#2-Zn(1)-O(8)#3	92.64(8)	O(3)-Zn(2)-O(6)#4	113.35(7)
O(3)-Zn(2)-N(3)	109.04(7)	O(6)#4-Zn(2)-N(3)	96.92(6)
O(10)-Zn(2)-O(3)	108.08(7)	O(10)-Zn(2)-O(6)#4	113.76(6)
O(10)-Zn(2)-N(3)	115.45(7)	N(1)-O(1)-Zn(1)	110.06(1)
N(2)-O(4)-Zn(1)	111.39(1)	N(4)-O(8)-Zn(1)#6	106.83(1)

Symmetric code：#1 -x+1, y, -z+3/2; #2 x, y+1, z; #3 -x+1, y+1, -z+3/2; #4 -x+1, -y+1, -z+1; #5 -x, -y+1, -z+1; #6 x, y-1, z.

2. Structures and characterization of Zn-MOF and Zn-MOF/GO
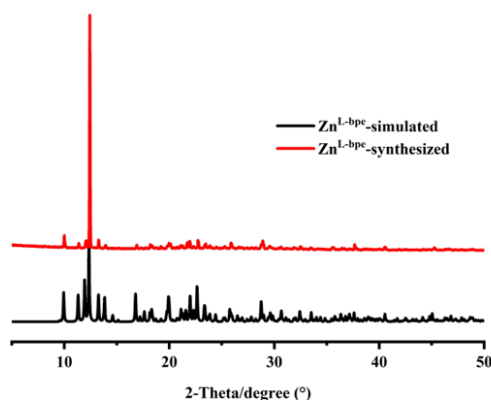
Fig. S1 The PXRD pattern of Zn^{L-bpe}.
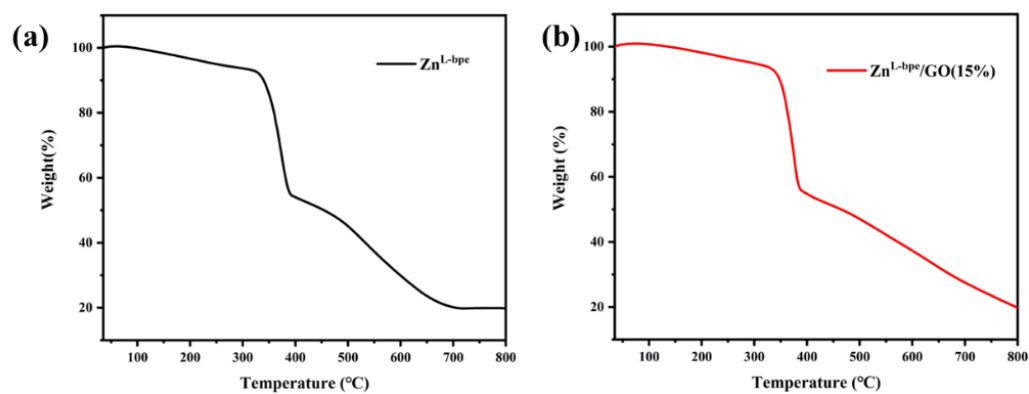
Fig. S2 The TG curves of Zn^{-L-bpe} and Zn^{-L-bpe}/GO(15%).
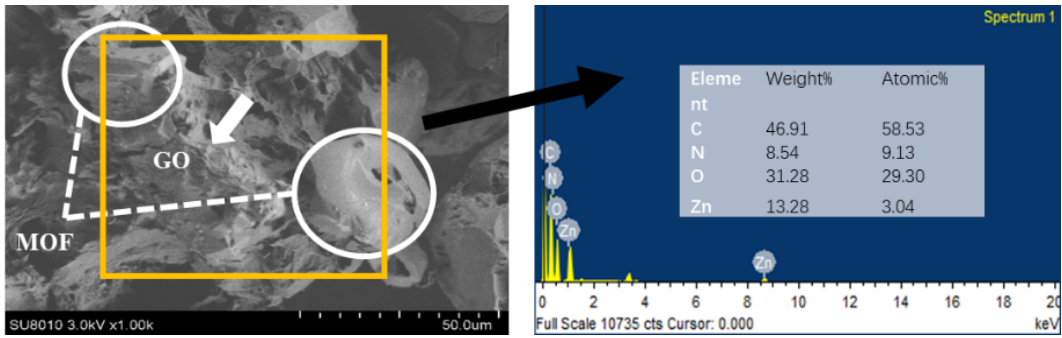
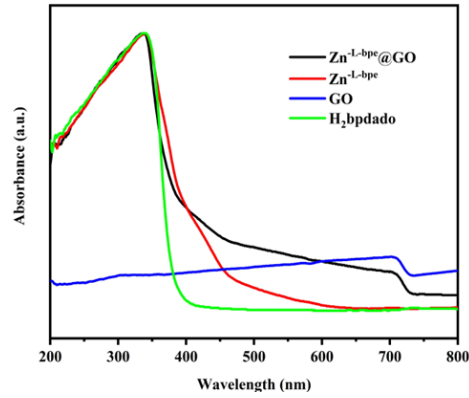**Fig. S3** The SEM images of Zn^{L-bpe}/GO(15%)

Fig. S4 The UV-vis spectra of H$_2$L, Zn^{L-bpe}, GO and Zn^{L-bpe}/GO(15%).
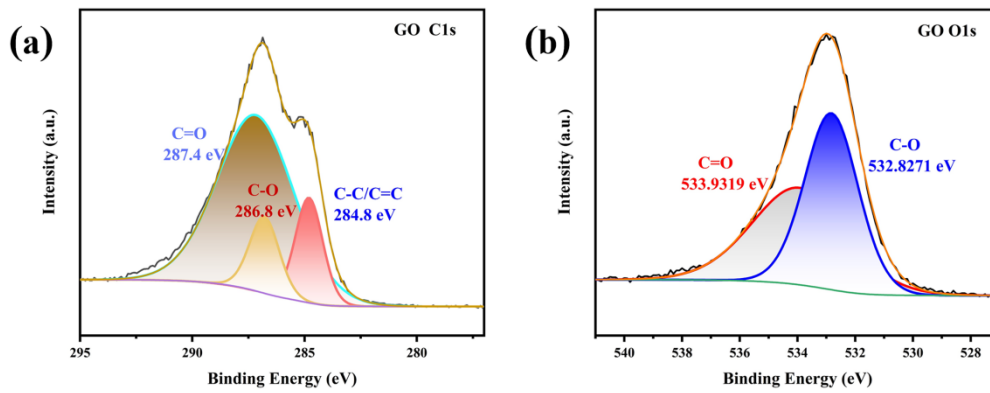

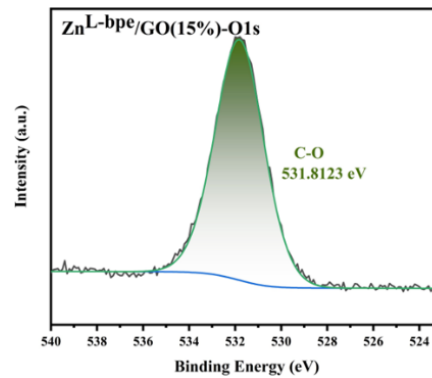**Fig. S5** The XPS spectra of C1s (a) and O1s (b) spectrum of GO.

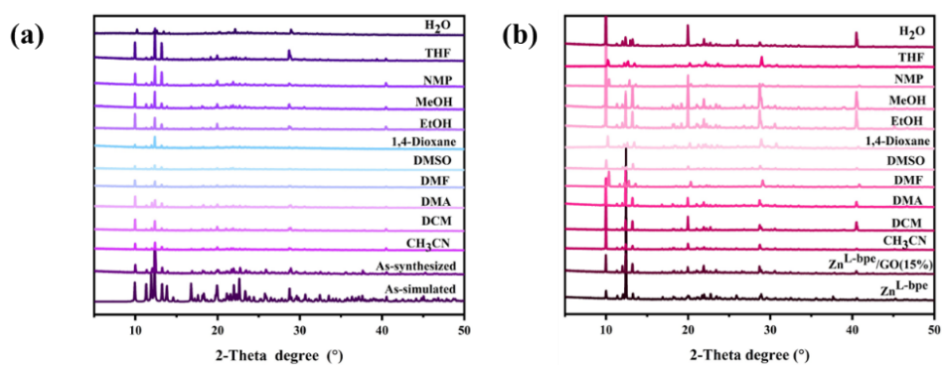**Fig. S6** The XPS spectra of O1s spectrum of Zn^{L-bpe}/GO(15%).

Fig. S7 Solvent stability analysis of the Zn^{L-bpe} and $Zn^{L-bpe}/GO(15\%)$.
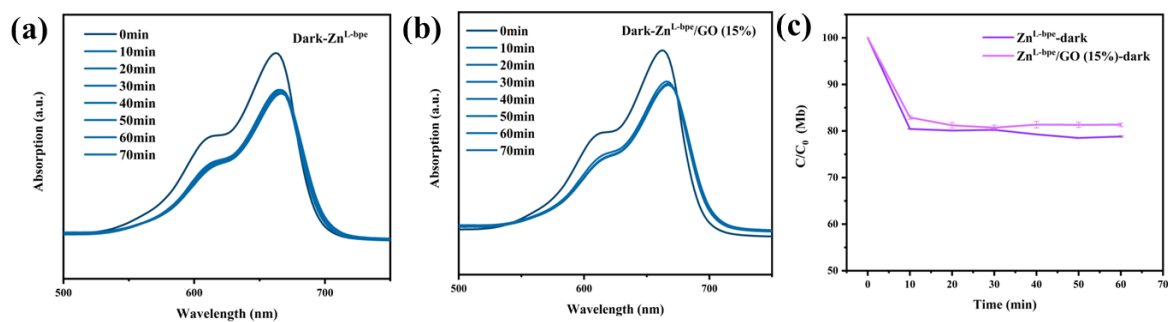
3. Photocatalytic decoloration of Mb

Fig. S8 The adsorption-desorption equilibrium of Zn^{L-bpe} and Zn^{L-bpe}/GO (15%) within 10 min towards Mb removal.
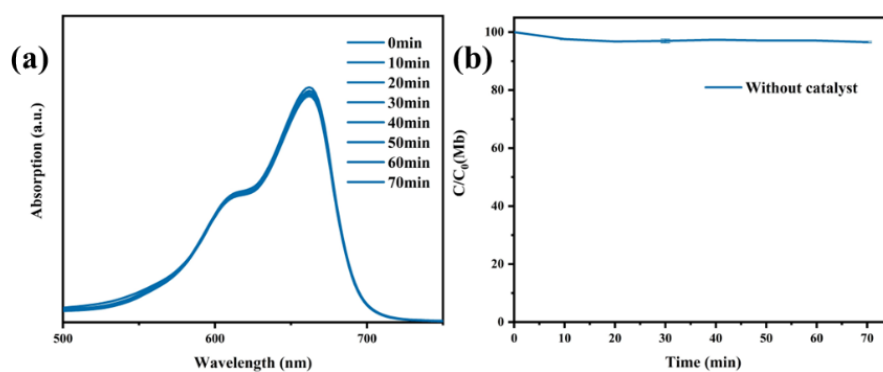
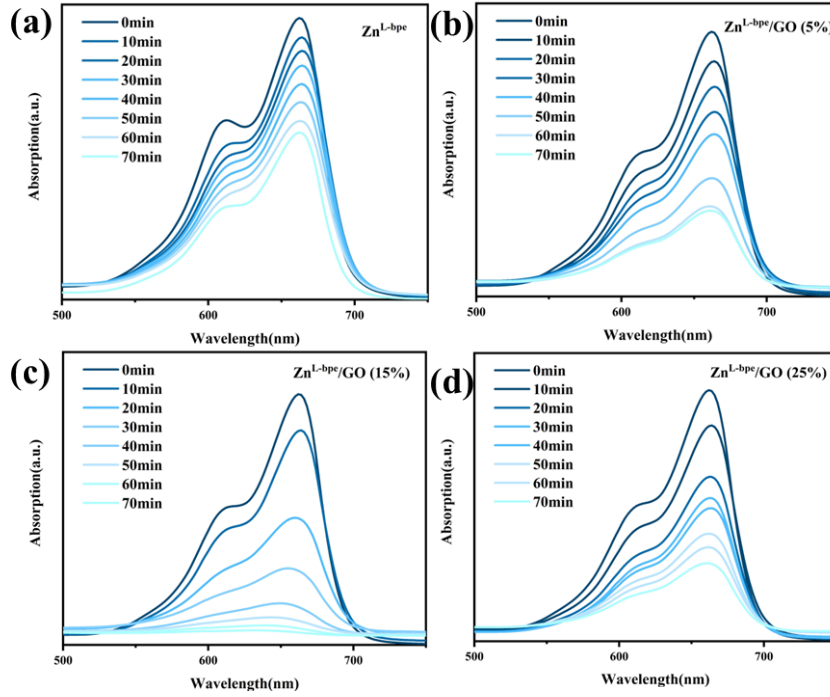**Fig. S9** View of the Mb removal without catalysts.

Fig. S10 The photocatalytic effect of different loads within 70 min towards Mb removal.
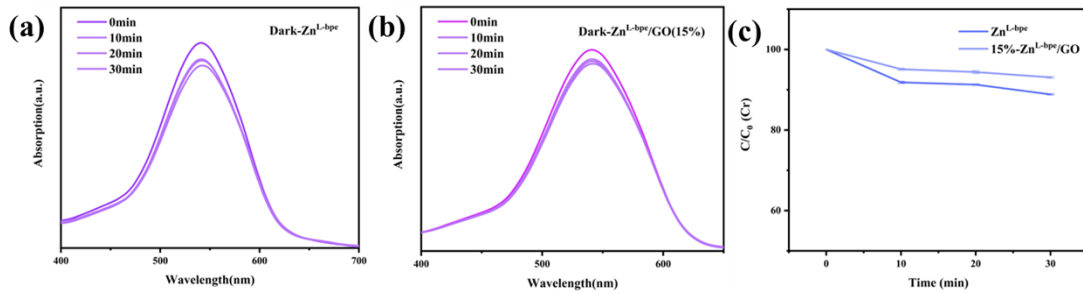
4. Photocatalytic reduction of Cr(VI)

Fig. S11 The adsorption-desorption equilibrium of Zn^{L-bpe} and $Zn^{L-bpe}/GO(15\%)$ within 10 min towards Cr(VI) removal.
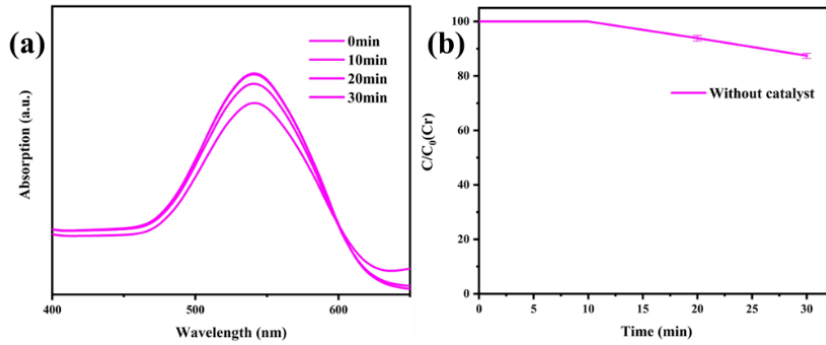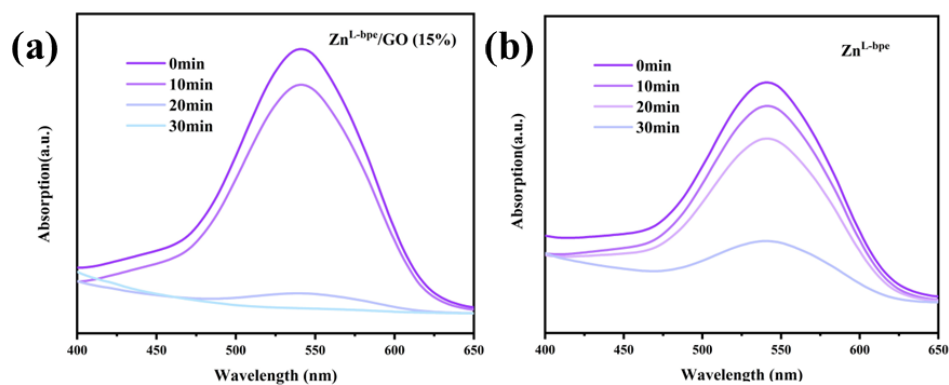

Fig. S12 View of the Mb removal without catalysts.

Fig. S13 The photocatalytic effect of Zn$^{L\text{-bpe}}$ and Zn$^{L\text{-bpe}}$/GO(15%) within 30 min towards Cr(VI) removal.
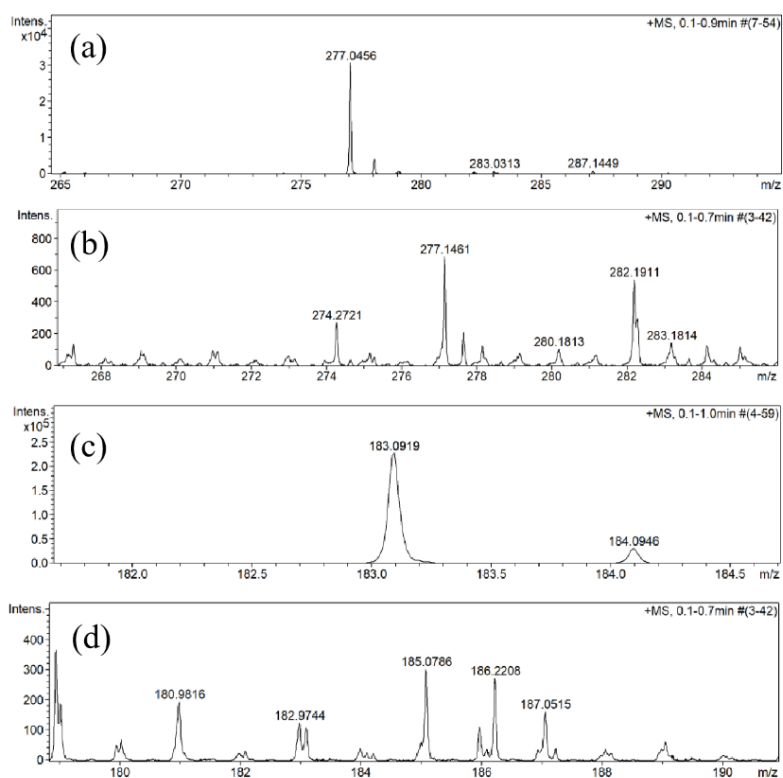

Fig. S14 The HRMS analysis of L (a) and bpe (c) and the reaction filtrate (b) and (d) for the second cycle (L: [M+H]: calcd. 277.0455. bpe: [M+H]: calcd.183.0916]
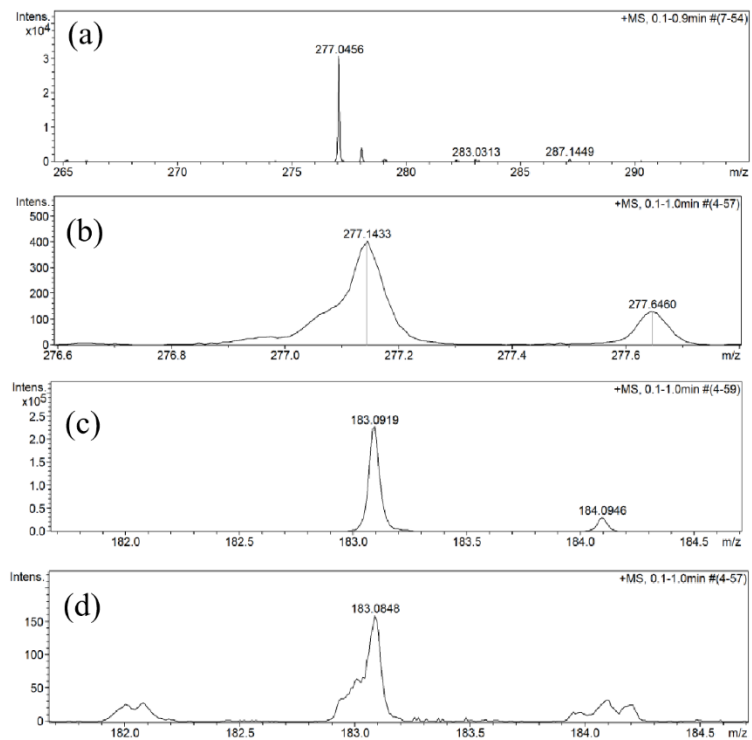
Fig. S15 The HRMS analysis of L (a) and bpe (c) and the reaction filtrate (b) and (d) for the third cycle (L: [M+H]: calcd. 277.0455. bpe: [M+H]: calcd. 183.0916]
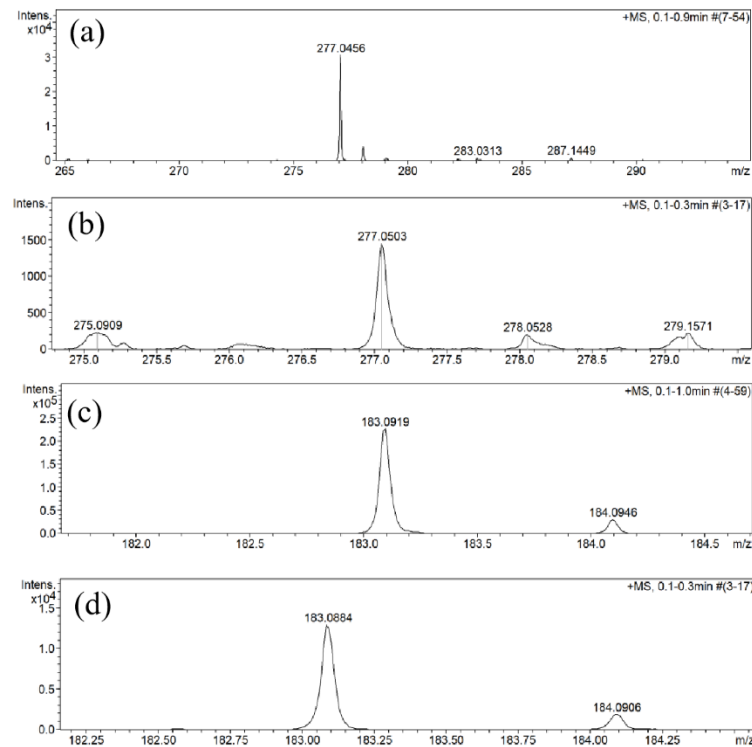

Fig. S16 The HRMS analysis of L (a) and bpe (c) and the reaction filtrate (b) and (d) for the fourth cycle (L: [M+H]: calcd. 277.0455. bpe: [M+H]: calcd. 183.0916]

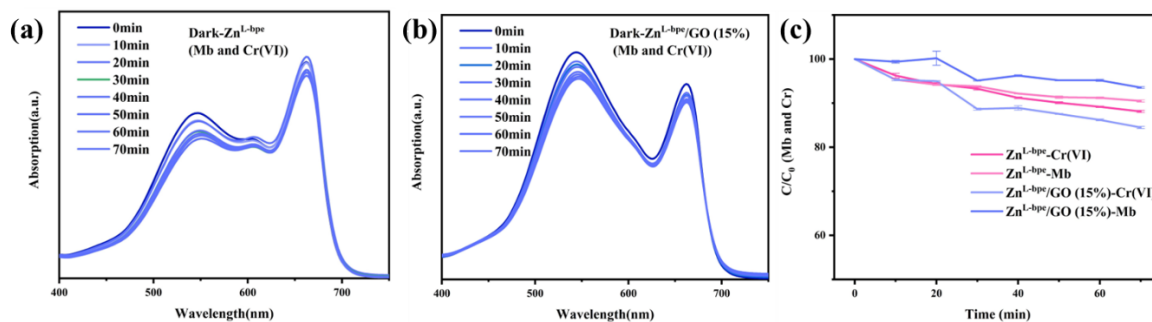## 5. Photocatalytic simultaneous removal of Cr(VI) and Mb

Fig. S17 The adsorption-desorption equilibrium of Zn^{L-bpe} and $Zn^{L-bpe}/GO(15\%)$ within 10 min towards Cr(VI) and Mb removal.
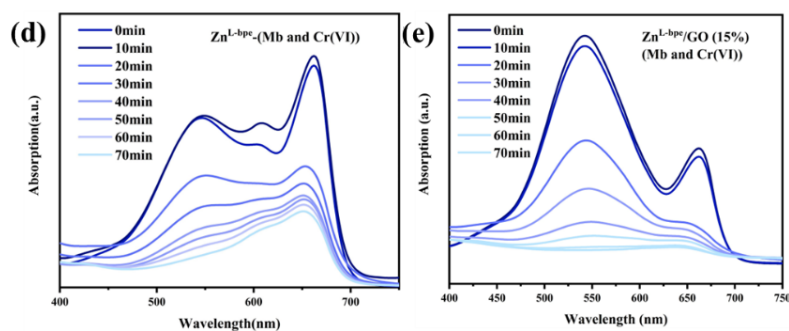

Fig. S18 The photocatalytic effect of Zn^{L-bpe} and $Zn^{L-bpe}/GO(15\%)$ within 70 min towards Mb and Cr(VI) removal.

Table S3. Comparation of simutaneous photocatalytic removal efficiency between different materials.

PhotocatalystsAmount(mg)	Solutions/Volume(mL) /concentration (ppm)	Time/min	Removal efficiency (%)	Ref
Zn^{L-bpe}/GO (15%)	Mb/10/20 Cr (VI)/10/40	70	87.9 99.8	This study
2D·MoS2/RP/50.	RhB /100/10 Cr (VI)/100/40	80	97.5/ 72.7	[1]
BiOI/GO/Bi2S3/50.	Phenol./50/10 Cr (VI)/50/50	240	95 70	[2]
Cunanoparticles'sensitized.TiO₂, nanotube arrays	RhB/50/20 Cr (VI)/20/10	120	95.7 45	[3]
CdS·ODs-Doped: yBizMo0./.20	Phenol/20/10 Cr(VI)/20/100	60	47 97	[4]
MOC@COF-2	TC/10/10 Cr(VI)/10/10	120	95 97	[5]
TBD	Cr(VI)/50/100 MO/50/100	/	91.29 82.84	[6]

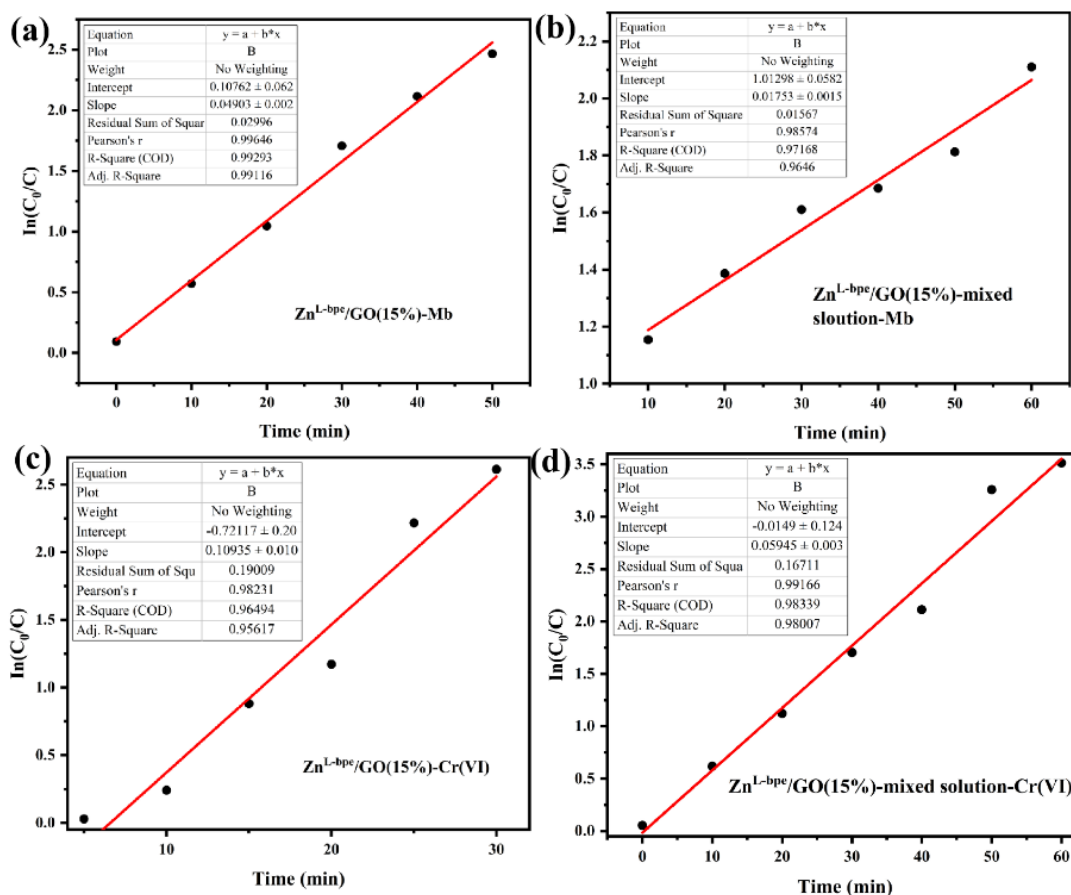**Fig. S19** The pseudo-first-order reaction of $Zn^{L-bpe}/GO(15\%)$ towards the removal of Mb (a), Cr(VI) (c), and the Mb (b) and Cr(VI) (d) in the coexistence of Mb and Cr(VI) in deionized water.
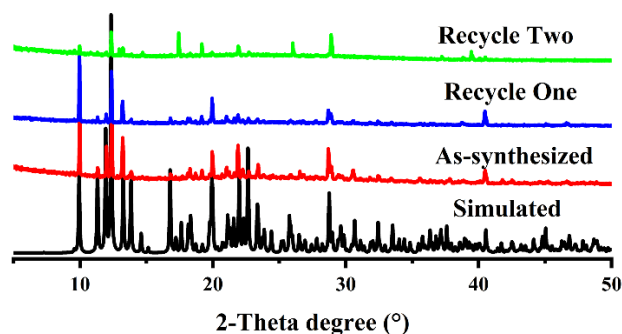

Fig. S20 The PXRD of $Zn^{L-bpe}/GO(15\%)$ recovered from the reaction solution upon simultaneously removing the Mb and Cr(VI).
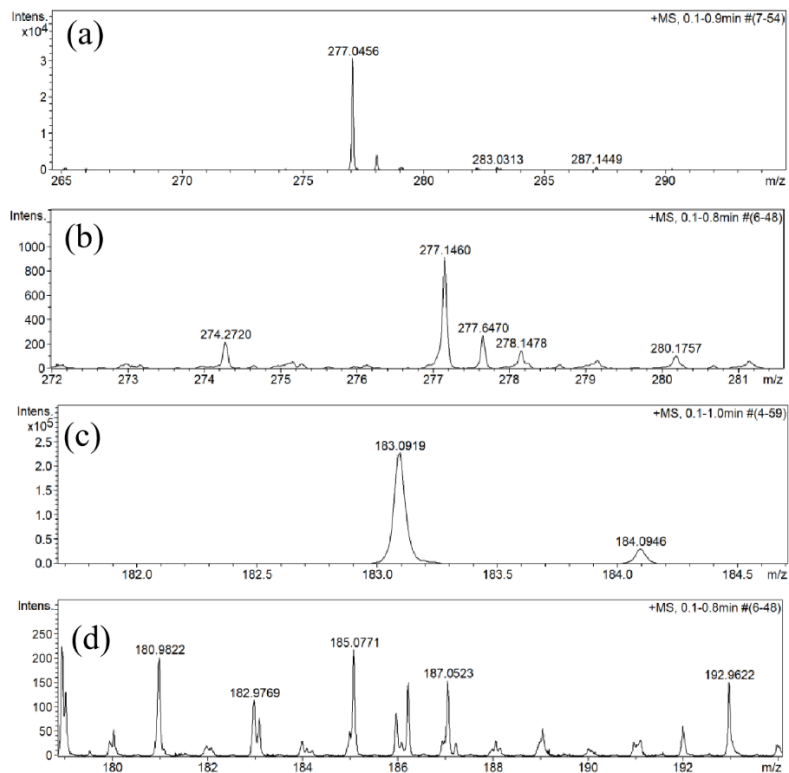
Fig. S21 The HRMS analysis of L (a) and bpe (c) and the reaction filtrate (b) and (d) for the second cycle upon simultaneously removing the Mb and Cr(VI) (L: [M+H]: calcd. 277.0455. bpe: [M+H]: calcd. 183.0916]

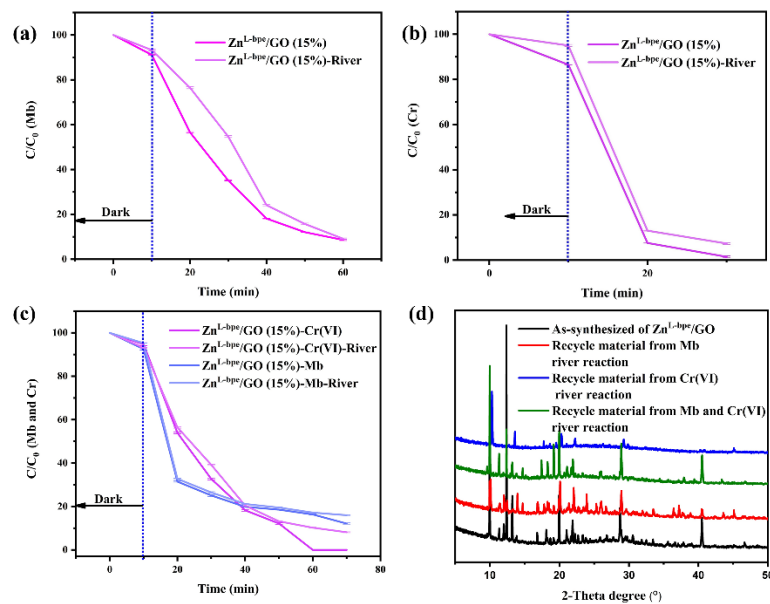## 6. Photocatalytic removal of Cr(VI) or/and Mb in Feng-river

Fig. S22 The Mb (a) and Cr(VI) (b) removal for $Zn^{L-bpe}/GO(15\%)$ in Feng-river; (c) The simultaneous removal of Cr(VI) and Mb for $Zn^{L-bpe}/GO(15\%)$ in Feng-river; (d) The PXRD of $Zn^{L-bpe}/GO(15\%)$ recovered from river water.

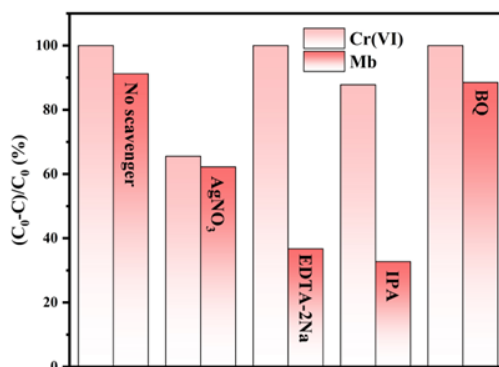# 7. Mechanism of photodegradation performance enhancement

Fig. S23 The photocatalytic degradation efficiency for Zn-L-bpe/GO(15%) towards the removal of Cr(VI) and Mb with various scavengers of active species;
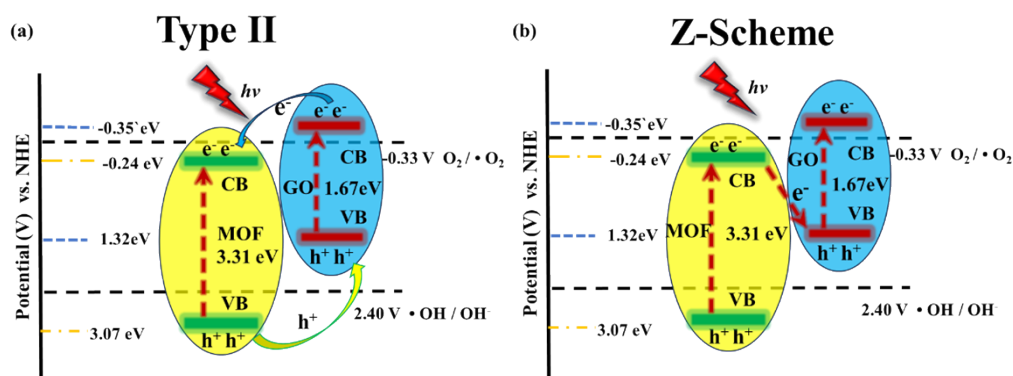

Fig. S24 (a) A hypothetical type-II heterojunction model of $Zn^{L-bpe}/GO(15\%)$; (b) View of Z-Scheme $Zn^{L-bpe}/GO(15\%)$ heterojunction.

8. References

[1]Bai X.,Wan J., Jia J., et al., Simultaneous photocatalytic removal of Cr(VI) and RhB over 2D MoS_2/Red phosphorus heterostructure under visible light irradiation. *Materials Letters* **2018,** *222*, 187-191.

[2]Chen A., Bian Z., Xu J., et al., Simultaneous removal of Cr(VI) and phenol contaminants using Z-scheme bismuth oxyiodide/reduced graphene oxide/bismuth sulfide system under visible-light irradiation. *Chemosphere* **2017,** *188*, 659-666.

[3]Zhong J. S., Wang Q. Y., Zhou J., et al., Highly efficient photoelectrocatalytic removal of RhB and Cr(VI) by Cu nanoparticles sensitized TiO_2 nanotube arrays. *Applied Surface Science* **2016,** *367*, 342-346.

[4]Kandi D., Martha S., Thirumurugan A., et al., CdS QDs-Decorated Self-Doped γ-Bi_2MoO_6: A Sustainable and Versatile Photocatalyst toward Photoreduction of Cr(VI) and Degradation of

Phenol. *ACS Omega* **2017,** *2* (12), 9040-9056.

[5]Qi L., Zhou Y., Qi J., et al., Enhanced Generation and Effective Utilization of Cr(V) for Simultaneous Removal of Coexisting Pollutants via MOF@COF Photocatalysts. *ACS ES&T Engineering* **2024**, doi: 10.1021/acsestengg.3c00491.

[6]Zhao J., Yang X., Yang Y., et al., Biomass polyamine-functionalized nanocellulose-loaded covalent organic framework to construct composite aerogels for highly efficient removal of Cr (VI) and methyl orange. *Chemical Engineering Journal* **2024,** *486*, 150282.